



General-Variable Order Fractional Creep Constitutive Model for Cemented Backfill Materials: Considerations of Particle Size, Dosage, and Confining Pressure



Jiangyu Wu^{1,2,3}, Yiyi Feng^{4*}, Yiming Wang¹, Hongwen Jing¹, Hai Pu¹, Qian Yin¹, Dan Ma⁵

¹ State Key Laboratory for Geomechanics and Deep Underground Engineering, China University of Mining and Technology, 221116 Xuzhou, China

² State Key Laboratory of High Performance Civil Engineering Materials, Jiangsu Research Institute of Building Science Co., Ltd., 210008 Nanjing, China

³ Department of Materials, University of Oxford, Parks Rd, OX1 3PH Oxford, UK

⁴ Research Center of Dynamical Systems and Control, Soochow University, 234000 Suzhou, China

⁵ School of Mines, China University of Mining and Technology, 221116 Xuzhou, China

* Correspondence: Yiyi Feng (yyfeng12cumt@163.com)

Received: 10-26-2023

Revised: 11-30-2023

Accepted: 12-15-2023

Citation: J. Y. Wu, Y. Y. Feng, Y. M. Wang, H. W. Jing, H. Pu, Q. Yin, and D. Ma, "General-variable order fractional creep constitutive model for cemented backfill materials: Considerations of particle size, dosage, and confining pressure," *GeoStruct. Innov.*, vol. 1, no. 1, pp. 43–52, 2023. <https://doi.org/10.56578/gsi010104>.



© 2023 by the authors. Published by Acadlore Publishing Services Limited, Hong Kong. This article is available for free download and can be reused and cited, provided that the original published version is credited, under the CC BY 4.0 license.

Abstract: Building upon the foundations of classical fractional derivatives, the general fractional derivative emerges as a significant advancement in the development of constitutive models, especially for materials with complex properties. This derivative distinguishes itself through a kernel function of variable form, enabling it to encapsulate diverse characteristics of the creep process more effectively than its classical counterpart. This study introduces a general-variable order fractional creep constitutive model, ingeniously linking the order of the fractional derivative to Talbot gradation, which describes the aggregate gradation of cemented backfill materials, alongside dosage and confining pressure parameters. The model's innovative design synergizes the kernel function's diversity from the general fractional derivative with the phase adaptability inherent in the variable-order derivative. This integration permits a comprehensive description of each stage of the creep curve for cementitious filling materials in varying compositions, leveraging the Gamma function's properties within the positive real number domain. The model's rationality and validity are substantiated through a comparative analysis between experimental creep curves and theoretical predictions, affirming its relevance and accuracy in practical applications. This approach represents a notable contribution to the understanding of cemented backfill materials' behavior, offering a robust tool for engineering analysis and design.

Keywords: Cemented backfill materials; Variable order fractional derivatives; Creep constitutive model; Parameter sensitivity analysis

1 Introduction

Cemented backfill materials, predominantly utilized in mining, are recognized as eco-friendly solutions. These materials are composed of waste rock aggregates such as gangue, tailings, slag, and construction waste [1–4], various cementitious agents including cement, high water materials, cementitious powders, and alkali-activated cementitious materials [5–8], and are mixed and cured with water. Their widespread adoption not only fosters solid waste recycling, thereby mitigating environmental pollution resulting from accumulation [9–11], but also plays a crucial role in supporting overlying strata once introduced into the goaf, significantly enhancing the safety and stability of the goaf structure [12–15].

The ability of cemented backfill materials to effectively transmit the overburden load and control roof movement deformation and surface uneven settlement is predominantly determined by their mechanical properties [16, 17]. When these materials are employed in mining areas, they are subjected to a prolonged triaxial compression state, due to the roof and lateral coal pillars. Therefore, an in-depth study of their creep mechanical properties is vital for ensuring the safety and stability of underground and surface structures within mining areas. The fractional order

creep constitutive model has been demonstrated as a potent tool in analyzing the creep mechanical properties of these materials. Traditional studies on the constitutive model of cemented backfill materials often employ integral order derivatives to construct models with numerous components and complex structures. However, the integration of fractional derivatives into the viscous element not only simplifies model complexity and reduces computational load but also establishes a constitutive relationship capable of describing various mechanical properties of the material. Building upon Riemann-Liouville fractional calculus, Wu et al. [18] introduced a creep model utilizing fractional-order derivatives for the viscoelastic damage of salt rock, effectively capturing the nonlinear accelerated creep stage. Similarly, Xiang et al. [19] established a model where the fractional order correlates directly with stress levels, employing the Almeida fractional derivative in the fractional creep model for soft soil to depict varying deformation patterns under different stress conditions. Gao and Yin [20] proposed a variable fractional order rheological model to characterize the full-stage creep behavior of rocks, confirming that the creep strain rate could be deduced from the slope of the order function.

The advent of the general fractional derivative in recent years has broadened the scope of classical fractional derivatives, introducing variability to the solutions of corresponding equations. This expansion is exemplified by the k-Hilfer-Prabhakar fractional derivative, through which Feng et al. [21] developed a generalized fractional viscoelastic-plastic constitutive model. This model is noteworthy for its ability to encapsulate classical models within its framework. Further advancements include the application of the general fractional-order derivative operator, integrating the Miller-Ross kernel in the Liouville-Sonine context. This approach has been successfully employed in the Maxwell and Kelvin-Voigt models, yielding viscoelastic constitutive models characterized by their inherent properties of inheritance and memorability [22].

In this study, the focus is placed on the Talbot gradation, which delineates the particle size distribution in cementitious filling materials, alongside the dosage of cemented backfill materials and the confining pressure. These factors are identified as critical indicators in the fractional derivative of the creep constitutive model. Leveraging the distinct capabilities of the general-variable fractional derivative and the properties of the Gamma function, a fractional creep model is formulated. This model adeptly describes the creep process of cementitious filling materials under graded loading conditions. The structure of this study is outlined as follows: In Section 2, the Sonine general fractional derivative featuring a nonsingular kernel and the Laplace transform of this fractional calculus are introduced. Section 3 proposes a three-element creep constitutive model, accompanied by an analytical solution. The sensitivity analysis of model parameters, crucial for understanding the impact of variations in fractional derivatives, is presented in Section 4. The study culminates in Section 5, where the conclusions are succinctly outlined.

2 Sonine General Fractional Derivative with Nonsingular Kernel

The exploration of generalized fractional derivatives has led to the consideration of the Sonine general fractional derivative, which is characterized by a nonsingular kernel. This derivative stands out due to the adaptable nature of its kernel function. The subsequent subsections delineate the definition and properties of this fractional calculus.

Definition 2.1 ([23]). Let $1 \geq \alpha \geq 0$ and $\lambda \in R$.

The Sonine general fractional derivative is defined within the interval $[a, b]$. The left-sided derivative of this form is given by Eq. (1).

$$\begin{aligned} & sD_{a+}^{\alpha, \lambda} f(t) \\ &= \frac{d}{dt} \left({}_{SH}I_{a+}^{\alpha, \lambda} f \right) (t) \\ &= \frac{d}{dt} f_a^t S_2 (\lambda(t - \tau)^{\alpha+1}) f(\tau) d\tau \end{aligned} \quad (1)$$

where, ${}_{SH}I_{a+}^{\alpha, \lambda} f(t) = \int_a^t S_2 (\lambda(t - \tau)^{\alpha+1}) f(\tau) d\tau$.

Similarly, the right-sided derivative in the same interval is defined as per Eq. (2).

$$\begin{aligned} & sD_{b-}^{\alpha, \lambda} f(t) \\ &= -\frac{d}{dt} \left({}_{SH}I_{b-}^{\alpha, \lambda} f \right) (t) \\ &= -\frac{d}{dt} f_t^b S_2 (\lambda(\tau - t)^{\alpha+1}) f(\tau) d\tau \end{aligned} \quad (2)$$

where, ${}_{SH}I_{b-}^{\alpha, \lambda} f(t) = \int_t^b S_2 (\lambda(\tau - t)^{\alpha+1}) f(\tau) d\tau$, and the incorporation of a nonsingular kernel.

$$S_2 (\lambda t^\alpha) = \sum_{n=0}^{\infty} \frac{(-\lambda)^n t^{n+\alpha-1}}{\Gamma(n+1)\Gamma(n+\alpha)}$$

The Laplace transforms for both the integral and derivative forms of the Sonine general fractional calculus with a nonsingular kernel are presented.

Let $f(t) \in L_k(a, b)$ ($1 \leq \kappa \leq \infty$), $1 \geq \alpha \geq 0$, $\lambda \in R$ and $|\frac{\lambda}{s}| < 1$. Then

$$L\left\{{}_sI_{0+}^{\alpha, \lambda} f(t)\right\} = s^\alpha e^{\frac{\lambda}{s}} \tilde{f}(s) \quad (3)$$

and

$$L\left\{{}_sD_{0+}^{\alpha, \lambda} f(t)\right\} = s^{1-\alpha} e^{-\frac{\lambda}{s}} \tilde{f}(s) \quad (4)$$

where, the Laplace transform of function $f(t)$ is given by $L\{f(t)\} = \tilde{f}(s) = \int_0^\infty e^{-st} f(t) dt$.

3 General-Variable Fractional Constitutive Model

3.1 Talbot Gradation Dependent Fractional Constitutive Model

In the context of cemented backfill materials, the Talbot gradation, denoted as n , serves as a critical metric for describing the aggregate particle size distribution. It has been observed that the creep characteristics of these materials exhibit variation with different Talbot gradation values. Consequently, a variable order fractional creep constitutive model, which is responsive to the Talbot gradation n , is proposed. This model is formulated based on the Sonine general fractional derivative with a nonsingular kernel, as discussed in Section 2. It leverages the generalization property of the kernel function to effectively capture the gradation-dependent creep behavior.

The general-variable order of the Talbot gradation dependent fractional derivative $\beta(n)$ is defined according to Eq. (5).

$$\beta(n) = A_1 \Gamma(A_2 n) \quad (5)$$

This derivative utilizes the Gamma function, symbolized by $\Gamma(x) = \int_0^\infty e^{-t} \cdot t^{x-1} dt$, to describe the variations in the derivative of the fractional dashpot with Talbot gradation n within the creep constitutive model. For a given set of cemented backfill materials, the determination of parameters A_1 and A_2 consequently fixes the order $\beta(n)$ in the corresponding fractional creep constitutive model.

Figure 1 illustrates the Talbot gradation dependent general-variable order fractional creep constitutive model, composed of three elements: two springs (denoted as E_1 and E_2) and a fractional dashpot (ξ).

The constitutive equation for the Talbot gradation dependent general-variable order fractional creep constitutive model is derived from the series-parallel relationship of each element within the system. This derivation process is outlined below.

$$\begin{cases} \varepsilon(t) = \varepsilon_1(t) + \varepsilon_2(t) \\ \varepsilon_1(t) = \frac{\sigma(t)}{E_1} \\ {}_sD_{0+}^{\beta(n), \lambda} \varepsilon_2(t) + \frac{E_2}{\xi} \varepsilon_2(t) = \frac{\sigma(t)}{\xi} \\ \beta(n) = A_1 \Gamma(A_2 n) \end{cases} \quad (6)$$

When the axial load satisfies $\sigma(t) = \sigma_0 H(t)$, and utilizing the Laplace transform of the Sonine general fractional derivative with a nonsingular kernel, the equation is transformed into its Laplace domain representation, as shown in Eq. (7).

$$s^{1-\beta(n)} e^{-\frac{\lambda}{s}} \tilde{\varepsilon}_2(s) + \frac{E_2}{\xi} \tilde{\varepsilon}_2(s) = \frac{\sigma_0}{\xi} \frac{1}{s} \quad (7)$$

Further manipulation of Eq. (7) leads to its equivalent form in Eq. (8).

$$\tilde{\varepsilon}_2(s) = \frac{\sigma_0}{\xi} \frac{1}{s} \cdot \frac{1}{s^{1-\beta(n)} e^{-\frac{\lambda}{s}} + \frac{E_2}{\xi}} = \frac{\sigma_0 s^{-1}}{E_2 + \xi s^{1-\beta(n)} e^{-\frac{\lambda}{s}}} = \frac{\sigma_0}{E_2} \cdot \frac{s^{-1}}{1 + \frac{\xi}{E_2} e^{-\frac{\lambda}{s}} s^{1-\beta(n)}} \quad (8)$$

A noteworthy observation here is encapsulated in Eq. (9).

$$e^{-\frac{\lambda}{s}} = \sum_{m=0}^{\infty} \frac{1}{m!} \left(-\frac{\lambda}{s}\right)^m = \sum_{m=0}^{\infty} \frac{(-\lambda)^m}{m!} \cdot s^{-m} \quad (9)$$

Substituting Eq. (9) into Eq. (8) yields Eq. (10).

$$\tilde{\varepsilon}_2(s) = \frac{\sigma_0}{E_2} \cdot \frac{s^{-1}}{1 + \frac{\xi}{E_2} \sum_{m=0}^{\infty} \frac{(-\lambda)^m}{m!} \cdot s^{-m} \cdot s^{1-\beta(n)}} = \frac{\sigma_0}{E_2} \cdot \frac{s^{-1}}{1 + \frac{\xi}{E_2} \sum_{m=0}^{\infty} \frac{(-\lambda)^m}{m!} s^{1-m-\beta(n)}} \quad (10)$$

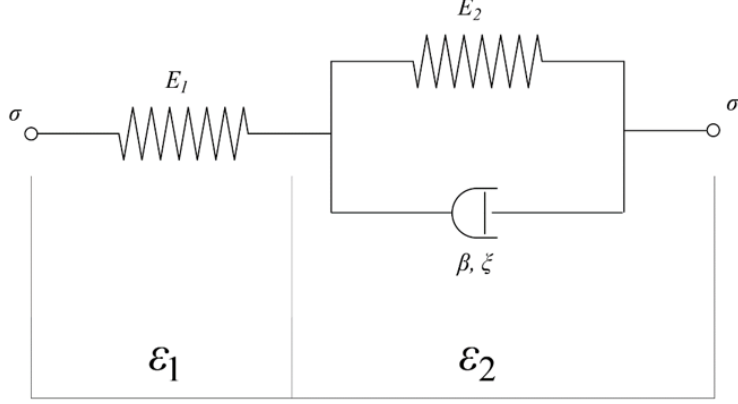


Figure 1. The Talbot gradation dependent general-variable order fractional creep constitutive model

When $m=0$, it results in Eq. (11).

$$\tilde{\varepsilon}_2(s) = \frac{\sigma_0}{E_2} \cdot \frac{s^{-1}}{1 + \frac{\xi}{E_2} s^{1-\beta(n)}} = \frac{\sigma_0}{E_2} \cdot \frac{s^{\beta(n)-2}}{\frac{1}{s^{1-\beta(n)}} + \frac{\xi}{E_2}} = \frac{\sigma_0}{E_2} \cdot \frac{E_2}{\xi} \cdot \frac{s^{\beta(n)-2}}{1 + \frac{E_2}{\xi} \frac{1}{s^{1-\beta(n)}}} \quad (11)$$

When $m \geq 1$, Eq. (12) becomes applicable.

$$\tilde{\varepsilon}_2(s) = \frac{\sigma_0}{E_2} \cdot \frac{s^{-1}}{1 + \frac{\xi}{E_2} \sum_{m=1}^{\infty} \frac{(-\lambda)^m}{m!} s^{1-m-\beta(n)}} \quad (12)$$

The strain, denoted as $\varepsilon_2(t)$, is derived from the inverse Laplace transform of Eqs. (11) and (12). This derivation is encapsulated in Eq. (13),

$$\varepsilon_2(t) = \begin{cases} \frac{\sigma_0}{\xi} \cdot t^{1-\beta(n)} \cdot M_{1-\beta(n), 2-\beta(n)} \left(-\frac{E_2}{\xi} t^{1-\beta(n)} \right), & m = 0 \\ \frac{\sigma_0}{E_2} \cdot \sum_{m=1}^{\infty} M_{m+\beta(n)-1} \left(-\frac{\xi}{E_2} \frac{(-\lambda)^m}{m!} t^{m+\beta(n)-1} \right), & m \geq 1 \end{cases} \quad (13)$$

where, $M_v(t) = \sum_{n=0}^{+\infty} \frac{t^n}{\Gamma(vn+1)}$ is the Mittag-Leffler function, $M_{v,z}(t) = \sum_{n=0}^{+\infty} \frac{t^n}{\Gamma(vn+z)}$ is the Wiman function.

The Laplace transforms of both the Mittag-Leffler and Wiman functions are provided.

$$\begin{aligned} L \{ M_v(\omega t^v) \} &= s^{-1} (1 - \omega^{-v})^{-1} \\ L \{ t^{z-1} M_{v,z}(\omega t^v) \} &= s^{-z} (1 - \omega^{-v})^{-1} \end{aligned}$$

Consequently, integrating Eqs. (6) and (14) yields a comprehensive constitutive relation for the Talbot gradation dependent general-variable order fractional creep constitutive model.

$$\begin{aligned} \varepsilon(t) &= \varepsilon_1(t) + \varepsilon_2(t) \\ &= \frac{\sigma_0 H(t)}{E_1} + \frac{\sigma_0}{\xi} \cdot t^{1-\beta(n)} \cdot M_{1-\beta(n), 2-\beta(n)} \left(-\frac{E_2}{\xi} t^{1-\beta(n)} \right), & m = 0 \\ &= \frac{\sigma_0 H(t)}{E_1} + \frac{\sigma_0}{E_2} \cdot \sum_{m=1}^{\infty} M_{m+\beta(n)-1} \left(-\frac{\xi}{E_2} \frac{(-\lambda)^m}{m!} t^{m+\beta(n)-1} \right), & m \geq 1 \end{aligned} \quad (14)$$

This relation, depicted in Eq. (14), is particularly notable for its correlation between the fractional order $\beta(n)$ and the Talbot gradation of the cemented backfill materials. In consideration of the solution's accuracy in practical calculations, $m \geq 1$ is adopted, ensuring the model's precision and reliability in real-world applications.

3.2 Dosage Dependent Fractional Constitutive Model

In the formulation of cemented backfill materials, the quantity of cemented material significantly impacts the compressive properties of the samples. Building on the general-variable fractional constitutive model established in Section 3.1, this segment of the study adapts the variable order derivative $\beta(n)$, initially related to Talbot gradation, to reflect the dosage of cemented backfill materials. This adaptation leads to the expression of the variable fractional order $\beta(m)$, as depicted in Eq. (15).

$$\beta(m) = A_1 \Gamma(A_2 m) \quad (15)$$

where, m represents the dosage of the cemented backfill materials.

The behavior of the Gamma function in the positive real number field, characterized by an initial decrease followed by an increase, enables the determination of the fractional derivative value for varying dosages of cemented backfill materials. This determination is facilitated by selecting appropriate parameters A_1 and A_2 .

Subsequently, the analytical solution of the dosage-dependent fractional constitutive model is derived, as shown in Eq. (16).

$$\varepsilon(t) = \frac{\sigma_0 H(t)}{E_1} + \frac{\sigma_0}{E_2} \cdot \sum_{i=1}^{\infty} M_{i+\beta(m)-1} \left(-\frac{\xi}{E_2} \frac{(-\lambda)^i}{i!} t^{i+\beta(m)-1} \right), i \geq 1 \quad (16)$$

where, m symbolizes the dosages of cemented backfill materials. This analytical solution is instrumental in understanding the material behavior under different dosage conditions, thereby enhancing the model's applicability in practical scenarios.

3.3 Confining Pressure Dependent Fractional Constitutive Model

Upon its transportation to the underground goaf, cemented backfill materials are subjected to pressures not only from the overlying strata but also from the surrounding rock mass. Recognizing the significance of confining pressure on the creep characteristics of these materials, this segment of the study develops a variable order fractional derivative model that reflects the confining pressure's influence.

The general-variable fractional derivative $\beta(\sigma_3)$, now adapted to incorporate confining pressure, is defined in Eq. (17).

$$\beta(\sigma_3) = A_1 \Gamma(A_2 \sigma_3) \quad (17)$$

Furthermore, the analytical solution of the confining pressure dependent fractional constitutive model is derived, as shown in Eq. (18).

$$\varepsilon(t) = \frac{\sigma_0 H(t)}{E_1} + \frac{\sigma_0}{E_2} \cdot \sum_{i=1}^{\infty} M_{i+\beta(\sigma_3)-1} \left(-\frac{\xi}{E_2} \frac{(-\lambda)^i}{i!} t^{i+\beta(\sigma_3)-1} \right), i \geq 1 \quad (18)$$

where, σ_3 symbolizes the confining pressure. This solution is integral to understanding the behavior of cemented backfill materials under different confining pressure scenarios, thereby enhancing the model's applicability and relevance in practical engineering contexts.

4 Model Verification with Different Creep Conditions

To verify the efficacy of the general-variable fractional creep constitutive model developed in this study, creep test data of cemented backfill materials under varying conditions of confining pressure, dosage, and particle size were utilized. These data, sourced from Wu et al. [24], encompassed different levels of confining pressure, with each level maintained for a duration of 7,200 seconds. The process of model verification involved the utilization of the particle swarm optimization theory [25] for fitting the creep test data under three distinct conditions.

4.1 Talbot Gradation of Cemented Backfill Materials

Specifically, the application of this optimization algorithm enabled the inverse modeling of Eq. (14) to determine the model parameters for cemented backfill materials with different Talbot gradations. The outcomes of this parameter fitting are presented in Table 1, showcasing results for varying Talbot gradations.

Subsequent to the parameter inversion, Figure 2 illustrates a comparison between the fitting curves and the experimental data for different Talbot gradations.

This comparison in Figure 2 reveals that the proposed Talbot gradation dependent general-variable order fractional creep constitutive model aligns closely with the experimental data across all graded loading levels, particularly during the stable creep stage. The fractional order $\beta(n)$ is determined by parameters A_1 and A_2 , and the Talbot gradation n . Through variations in these parameters, the model adeptly describes both the steady-state and accelerated creep stages of the materials.

4.2 Dosages of Cemented Backfill Materials

According to Eq. (15), the inversion results for different dosages of cemented backfill materials (specifically, 30 g and 50 g) are shown in Table 2.

Following the parameter inversion in Table 2, Figure 3 offers a comparative analysis between the fitting curves and the experimental creep data for the specified dosages.

Table 1. Parameter fitting results of different Talbot gradations

| n | σ/MPa | E_1/MPa | E_2/MPa | $\xi/\text{MPa} \cdot t^{\beta(n)}$ | A_1 | A_2 | λ |
|-----|---------------------|------------------|------------------|-------------------------------------|--------|--------|-----------|
| 0.2 | 1.0186 | 302.9334 | 587.2305 | 23.0871 | 0.2816 | 3.2356 | 1.0298 |
| | 2.0372 | 240.9110 | 617.3541 | 50.7389 | 0.0328 | 5.5890 | 6.3642 |
| | 1.0186 | 378.9657 | 690.0038 | 33.4310 | 0.2903 | 2.6932 | 2.5829 |
| 0.4 | 2.0372 | 106.1042 | 782.9204 | 34.2321 | 0.3738 | 4.1375 | 3.8460 |
| | 3.0557 | 210.3779 | 759.1121 | 56.2093 | 0.5593 | 3.3326 | 4.8364 |
| | 1.0186 | 218.4625 | 691.5732 | 28.7540 | 0.2249 | 1.3027 | 5.0310 |
| 0.6 | 2.0372 | 338.1249 | 774.2184 | 41.4521 | 0.4172 | 3.2147 | 4.9266 |
| | 3.0557 | 372.0438 | 802.1829 | 48.3369 | 0.4902 | 3.9462 | 3.7820 |
| | 4.0744 | 396.7476 | 854.6280 | 60.3267 | 0.3384 | 4.6034 | 5.3264 |
| 0.8 | 1.0186 | 311.3543 | 593.0239 | 30.2496 | 0.3924 | 3.8876 | 3.2902 |
| | 2.0372 | 281.4059 | 729.9800 | 34.9572 | 0.3019 | 5.0011 | 5.2939 |
| | 3.0557 | 243.5014 | 830.2848 | 50.2486 | 0.2802 | 5.9824 | 7.3892 |

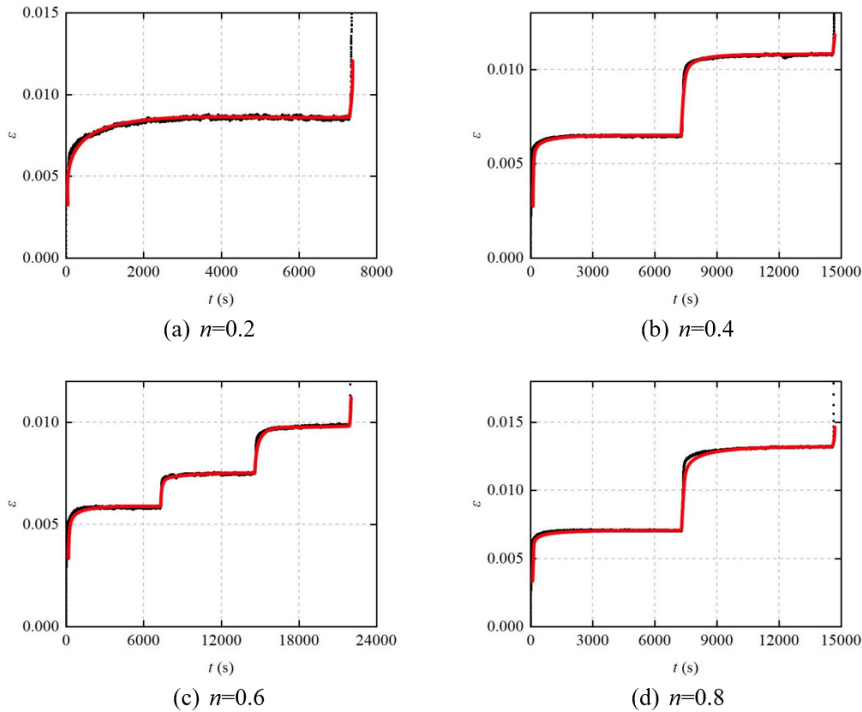


Figure 2. Comparison between fitting curves and experimental data

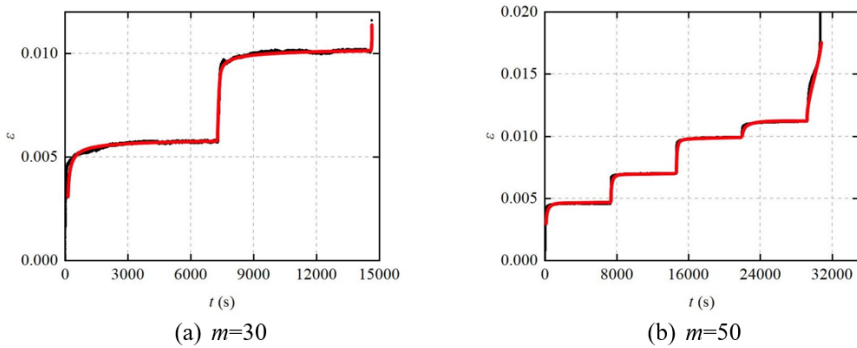


Figure 3. Comparison between fitting curves and experimental data

Notably, the model exhibits heightened accuracy in fitting the creep curve during the acceleration stage, especially when the curve presents a complete three-stage progression. This observation is evident from both Table 2 and Figure 3, underscoring the model's effectiveness in capturing the nuanced creep behavior of cemented backfill

materials under varied dosages.

4.3 Influence of Confining Pressures

This section examines the accuracy of the analytical solution (Eq. (18)) in describing the creep behavior of cemented backfill materials under various confining pressures and graded loading conditions. The inversion of parameters within the constitutive equation was facilitated by the particle swarm optimization algorithm, with the results tabulated in Table 3. This table enumerates the fitting outcomes for different levels of confining pressure.

The simulation curves, derived from the parameters listed in Table 3 and applied to Eq. (18), were compared against the actual test curves. Figure 4 presents this comparison, illustrating the model's performance under confining pressures of 0.5 MPa and 1.0 MPa.

An assessment of the fitting results from the three distinct types of general-variable fractional constitutive models reveals that the model proposed in this study aligns well with the creep test data of cemented backfill materials under step loading conditions. Notably, the model achieves high accuracy in both the steady-state and accelerated creep stages. This accuracy is maintained across variable fractional orders, whether these are associated with Talbot gradation, dosage, or confining pressure.

Table 2. Parameter fitting results of different dosages

| m | σ/MPa | E_1/MPa | E_2/MPa | $\xi/\text{MPa} \cdot t^{\beta(m)}$ | A_1 | A_2 | λ |
|----|---------------------|------------------|------------------|-------------------------------------|--------|--------|-----------|
| 30 | 1.0186 | 257.7429 | 547.4420 | 28.6774 | 0.3644 | 3.9181 | 1.6901 |
| | 2.0372 | 332.8758 | 650.5384 | 30.9917 | 0.4443 | 1.9675 | 0.9782 |
| | 3.0557 | 297.9427 | 763.2307 | 41.5799 | 0.3683 | 4.0225 | 3.9477 |
| | 1.0186 | 312.8474 | 423.9527 | 32.7373 | 0.2573 | 1.1282 | 2.8428 |
| | 2.0372 | 406.3348 | 550.1291 | 25.4130 | 0.1886 | 1.9156 | 3.5628 |
| 50 | 3.0557 | 427.9919 | 781.5589 | 34.8091 | 0.2581 | 2.2719 | 9.5182 |
| | 4.0744 | 413.4096 | 844.0744 | 46.5999 | 0.6017 | 4.5461 | 3.5481 |
| | 5.0930 | 429.2023 | 883.2696 | 50.2390 | 0.2145 | 2.0914 | 7.4789 |

Table 3. Parameter fitting results of different confining pressures

| σ_3/MPa | σ/MPa | E_1/MPa | E_2/MPa | $\xi/\text{MPa} \cdot t^{\beta(\sigma_3)}$ | A_1 | A_2 | 2 |
|-----------------------|---------------------|------------------|------------------|--|--------|--------|----------|
| 0.5 | 1.0186 | 426.3352 | 221.2362 | 31.1442 | 0.0613 | 7.1978 | 6.5475 |
| | 2.0372 | 362.9755 | 346.4261 | 26.7709 | 0.4417 | 1.1166 | 0.7568 |
| | 3.0557 | 389.0529 | 655.7584 | 29.1977 | 0.2305 | 3.8174 | 5.6515 |
| | 4.0744 | 343.4689 | 736.7183 | 10.3657 | 0.2418 | 7.1278 | 0.7614 |
| | 1.0186 | 474.8718 | 318.4161 | 22.1606 | 0.3995 | 4.4238 | 3.3817 |
| 1.0 | 2.0372 | 572.7942 | 483.2769 | 19.0734 | 0.7242 | 2.8217 | 1.2893 |
| | 3.0557 | 412.2144 | 590.3055 | 28.2773 | 0.1398 | 6.8423 | 4.5657 |
| | 4.0744 | 307.5483 | 783.9642 | 51.3190 | 0.7852 | 0.6384 | 6/6554 |
| | 5.0930 | 241.9477 | 984.0949 | 27.5482 | 0.0383 | 7.9349 | 3.1484 |

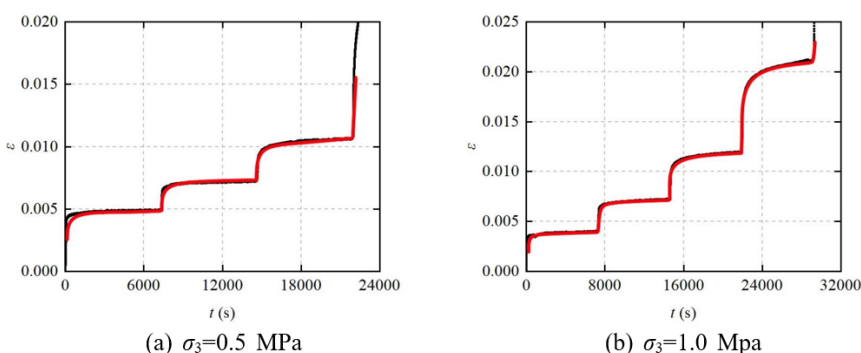


Figure 4. Comparison between fitting curves and experimental data

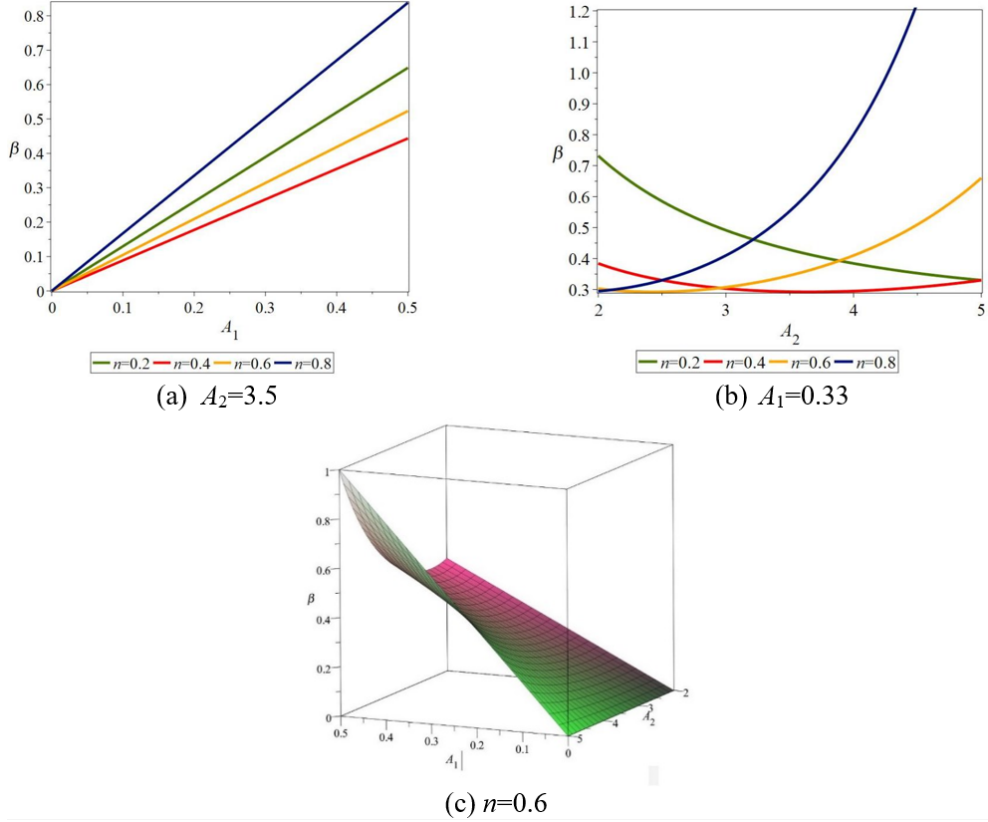


Figure 5. Plots of the fractional order

5 Sensitivity Analysis of Model Parameters A_1 and A_2

This section delves into the sensitivity of the crucial parameters A_1 and A_2 within the fractional order $\beta(n)$, as inferred from the inversion results detailed in Table 1. Subgraph (a) of Figure 5 illustrates the variation curve of the fractional order $\beta(n)$ in the constitutive model for cemented backfill materials with four different Talbot gradations, specifically when $A_2 = 3.5$ and $A_1 \in (0, 0.5)$. In a similar vein, subgraph (b) of Figure 5 depicts the change curve of $\beta(n)$ when $A_2 \in (2, 5)$ and $A_1 = 0.33$. Additionally, subgraph (c) of Figure 5 presents a three-dimensional representation of $\beta(n)$ when $A_1 \in (0, 0.5)$ and $A_2 \in (2, 5)$.

An analysis of the plots in Figure 5 indicates that the Talbot gradation n significantly influences the derivative order in the fractional creep constitutive model. It is observed that when A_1 and A_2 are fixed, the fractional order $\beta(n)$ corresponding to Talbot gradations of 0.4 and 0.6 is relatively small. This finding suggests that the value of $\beta(n)$ can be effectively fine-tuned by appropriately adjusting the parameters A_1 and A_2 in practical applications. Such an adjustment is crucial for optimizing the model's applicability and accuracy in real-world scenarios.

6 Conclusions

This study highlights that the creep curve of cemented backfill materials manifests in three distinct stages, a complexity not fully encapsulated by basic integral order constitutive models. To address this, a novel approach has been adopted, wherein Talbot gradation, dosage, and confining pressure are integrated as variables in the fractional derivative. This integration establishes a relationship between these variables and the strain-time curve, enhancing the model's capability to accurately depict the creep process in cementitious filling materials under varied conditions.

The Sonine general fractional derivative, characterized by a nonsingular kernel function, has been utilized to construct a generalized variable order fractional creep constitutive model. The analytical solution of this model's constitutive equation has been derived using the Laplace transform, its inverse, and the extended Mittag-Leffler function. The reliability and applicability of the proposed model are corroborated through a parameter inversion analysis, demonstrating its efficacy in fitting and analyzing the creep curves of cemented backfill materials. The model's adaptability to different particle sizes, dosages, and confining pressures makes it a valuable tool in practical engineering applications, providing a nuanced understanding of the creep behavior of these materials.

Author Contributions

Jiangyu Wu: Conceptualization, Methodology, Writing - review & editing. Yiyi Feng: Investigation, Methodology, Writing - original draft, Software. Yiming Wang: Data curation, Writing - review & editing. Hongwen Jing: Visualization, Supervision. Hai Pu: Data Curation, Validation, Resources. Qian Yin: Validation, Investigation. Dan Ma: Formal analysis, Writing - review & editing.

Data Availability

Data is available on request due to privacy restrictions.

Acknowledgements

This work was supported by the National Natural Science Foundation of China (42372328, 52122404, 52174092, 52074259, 52374147), Natural Science Foundation of Jiangsu Province, China (BK20220157), Xuzhou Science and Technology Project (KC22005).

Conflicts of Interest

The authors declare that they have no known competing financial interests or personal relationships that could have appeared to influence the work reported in this paper.

References

- [1] Z. F. Bian, X. X. Miao, S. G. Lei, S. E. Chen, W. F. Wang, and S. Struthers, “The challenges of reusing mining and mineral-processing wastes,” *Science*, vol. 337, no. 6095, pp. 702–703, 2012. <https://doi.org/10.1126/science.1224757>
- [2] J. Y. Wu, H. W. Jing, Q. Yin, L. Y. Yu, B. Meng, and S. C. Li, “Strength prediction model considering material, ultrasonic and stress of cemented waste rock backfill for recycling gangue,” *J. Clean. Prod.*, vol. 276, p. 123189, 2020. <https://doi.org/10.1016/j.jclepro.2020.123189>
- [3] S. Cao, E. Yilmaz, Z. Y. Yin, G. L. Xue, W. D. Song, and L. J. Sun, “CT scanning of internal crack mechanism and strength behavior of cement-fiber-tailings matrix composites,” *Cem. Concr. Compos.*, vol. 116, p. 103865, 2021. <https://doi.org/10.1016/j.cemconcomp.2020.103865>
- [4] D. Ma, H. Y. Duan, J. F. Liu, X. B. Li, and Z. L. Zhou, “The role of gangue on the mitigation of mining-induced hazards and environmental pollution: An experimental investigation,” *Sci. Total Environ.*, vol. 664, pp. 436–448, 2019. <https://doi.org/10.1016/j.scitotenv.2019.02.059>
- [5] X. Zhao, A. Fourie, and C. C. Qi, “Mechanics and safety issues in tailing-based backfill: A review,” *Int. J. Miner. Metall. Mater.*, vol. 27, pp. 1165–1178, 2020. <https://doi.org/10.1007/s12613-020-2004-5>
- [6] S. Y. Pan, Y. H. Chen, L. S. Fan, H. Kim, X. Gao, T. C. Ling, P. C. Chiang, S. L. Pei, and G. W. Gu, “CO₂ mineralization and utilization by alkaline solid wastes for potential carbon reduction,” *Nat. Sustain.*, vol. 3, pp. 399–405, 2020. <https://doi.org/10.1038/s41893-020-0486-9>
- [7] Q. S. Chen, Q. L. Zhang, C. C. Qi, A. Fourie, and C. C. Xiao, “Recycling phosphogypsum and construction demolition waste for cemented paste backfill and its environmental impact,” *J. Clean. Prod.*, vol. 186, pp. 418–429, 2018. <https://doi.org/10.1016/j.jclepro.2018.03.131>
- [8] E. Yilmaz, T. Belem, B. Bussire, and M. Benzaazoua, “Relationships between microstructural properties and compressive strength of consolidated and unconsolidated cemented paste backfills,” *Cem. Concr. Compos.*, vol. 33, pp. 702–715, 2011. <https://doi.org/10.1016/j.cemconcomp.2011.03.013>
- [9] H. B. Liu and Z. L. Liu, “Recycling utilization patterns of coal mining waste in China,” *Resour. Conserv. Recycl.*, vol. 54, no. 12, pp. 1331–1340, 2010. <https://doi.org/10.1016/j.resconrec.2010.05.005>
- [10] T. Zhu, W. J. Bian, S. Q. Zhang, P. K. Di, and B. S. Nie, “An improved approach to estimate methane emissions from coal mining in China,” *Environ. Sci. Technol.*, vol. 51, no. 21, pp. 12 072–12 080, 2017. <https://doi.org/10.1021/acs.est.7b01857>
- [11] Y. M. Wang, J. Y. Wu, and H. Pu, “Effect of calcium formate as an accelerator on dilatancy deformation, strength and microstructure of cemented tailings backfill,” *Chemosphere*, vol. 291, p. 132710, 2022. <https://doi.org/10.1016/j.chemosphere.2021.132710>
- [12] Y. L. Huang, J. M. Li, D. Ma, H. D. Gao, Y. C. Guo, and S. Y. Ouyang, “Triaxial compression behaviour of gangue solid wastes under effects of particle size and confining pressure,” *Sci. Total Environ.*, vol. 693, p. 133607, 2019. <https://doi.org/10.1016/j.scitotenv.2019.133607>
- [13] D. Ma, S. B. Kong, Z. H. Li, Q. Zhang, Z. H. Wang, and Z. L. Zhou, “Effect of wetting-drying cycle on hydraulic and mechanical properties of cemented paste backfill of the recycled solid wastes,” *Chemosphere*, vol. 282, p. 131163, 2021. <https://doi.org/10.1016/j.chemosphere.2021.131163>

- [14] S. Cao, G. L. Xue, E. Yilmaz, Z. Y. Yin, and F. D. Yang, “Utilizing concrete pillars as an environmental mining practice in underground mines,” *J. Clean. Prod.*, vol. 278, p. 123433, 2021. <https://doi.org/10.1016/j.jclepro.2020.123433>
- [15] J. Y. Wu, H. W. Jing, Y. Gao, Q. B. Meng, Q. Yin, and Y. Du, “Effects of carbon nanotube dosage and aggregate size distribution on mechanical property and microstructure of cemented rockfill,” *Cem. Concr. Compos.*, vol. 127, p. 104408, 2022. <https://doi.org/10.1016/j.cemconcomp.2022.104408>
- [16] E. Yilmaz, T. Belem, and M. Benzaazoua, “Effects of curing and stress conditions on hydromechanical, geotechnical and geochemical properties of cemented paste backfill,” *Eng. Geol.*, vol. 168, pp. 23–37, 2014. <https://doi.org/10.1016/j.enggeo.2013.10.024>
- [17] J. Y. Wu, H. W. Jing, Q. Yin, B. Meng, and G. S. Han, “Strength and ultrasonic properties of cemented waste rock backfill considering confining pressure, dosage and particle size effects,” *Constr. Build. Mater.*, vol. 242, p. 118132, 2020. <https://doi.org/10.1016/j.conbuildmat.2020.118132>
- [18] F. Wu, X. H. Zhou, P. Ying, C. B. Li, Z. M. Zhu, and J. Chen, “A study of uniaxial acoustic emission creep of salt rock based on improved fractional-order derivative,” *Rock Mech. Rock Eng.*, vol. 55, pp. 1619–1631, 2022. <https://doi.org/10.1007/s00603-021-02741-3>
- [19] G. J. Xiang, D. S. Yin, C. X. Cao, and Y. F. Gao, “Creep modelling of soft soil based on the fractional flow rule: Simulation and parameter study,” *Appl. Math. Comput.*, vol. 403, p. 126190, 2021. <https://doi.org/10.1016/j.amc.2021.126190>
- [20] Y. F. Gao and D. S. Yin, “A full-stage creep model for rocks based on the variable-order fractional calculus,” *Appl. Math. Model.*, vol. 95, pp. 435–446, 2021. <https://doi.org/10.1016/j.apm.2021.02.020>
- [21] Y. Y. Feng, X. J. Yang, J. G. Liu, and Z. Q. Chen, “Study on the generalized k-Hilfer–Prabhakar fractional viscoelastic–plastic model,” *Math. Mech. Solids.*, vol. 27, pp. 491–500, 2022. <https://doi.org/10.1177/10812865211025813>
- [22] Y. Y. Feng, X. J. Yang, J. G. Liu, and Z. Q. Chen, “Rheological analysis of the general fractional-order viscoelastic model involving the Miller–Ross kernel,” *Acta Mech.*, vol. 232, pp. 3141–3148, 2021. <https://doi.org/10.1007/s00707-021-02994-7>
- [23] N. Sonine, “On the generalization of an Abel formula (Sur la généralisation d'une formule d'Abel),” *Acta Math.*, vol. 4, pp. 171–176, 1884.
- [24] J. Y. Wu, H. W. Jing, Q. B. Meng, Q. Yin, and L. Y. Yu, “Assessment of cemented waste rock backfill for recycling gangue and controlling strata: Creep experiments and models,” *Environ. Sci. Pollut. Res.*, vol. 28, pp. 35 924–35 940, 2021. <https://doi.org/10.1007/s11356-021-12944-4>
- [25] C. C. Qi, A. Fourie, and Q. S. Chen, “Neural network and particle swarm optimization for predicting the unconfined compressive strength of cemented paste backfill,” *Constr. Build. Mater.*, vol. 159, pp. 473–478, 2018. <https://doi.org/10.1016/j.conbuildmat.2017.11.006>